Radiofluorination of A Highly Potent ATM Inhibitor As A Potential PET Imaging Agent

Claudia Fraser1
University of Oxford https://orcid.org/0000-0002-2979-3142
Javier Ajenjo
University of Oxford
Mathew Veal
University of Oxford
Gemma Dias
University of Oxford
Chung Chan
University of Oxford
Edward O'Neill
University of Oxford
Gianluca Destro
University of Oxford
Doreen Lau
University of Oxford
Anna Pacelli
University of Oxford
Veronique Gouverneur
University of Oxford
Rebekka Hueting
University of Oxford
Bart Cornelissen (bart.cornelissen@oncology.ox.ac.uk)
University of Oxford https://orcid.org/0000-0001-7581-3303

Research Article

Keywords: PET, ATM, cancer, molecular imaging

Posted Date: February 2nd, 2022

DOI: https://doi.org/10.21203/rs.3.rs-1228717/v1

Abstract

Purpose: Ataxia telangiectasia mutated (ATM) is a key mediator of the DNA damage response, and several ATM inhibitors (ATMi) are currently undergoing early phase clinical trials for the treatment of cancer. A radiolabelled ATMi to determine drug pharmacokinetics could assist patient selection in a move towards more personalised medicine. The aim of this study was to synthesise and investigate the first ^{18}F-labelled ATM inhibitor [^{18}F]**1** for non-invasive imaging of ATM protein and ATMi pharmacokinetics.

Methods: Radiofluorination of a confirmed selective ATM inhibitor (**1**) was achieved through substitution of a nitro-precursor with [^{18}F]fluoride. Uptake of [^{18}F]**1** was assessed *in vitro* in H1299 lung cancer cells stably transfected with shRNA to reduce expression of ATM. Blocking studies using several non-radioactive ATM inhibitors assessed binding specificity to ATM. *In vivo* biodistribution studies were performed in wild-type and ATM-knockout C57BL/6 mice using PET/CT and *ex vivo* analysis. Uptake of [^{18}F]**1** in H1299 tumour xenografts was assessed in BALB/c *nu/nu* mice.

Results: Nitro-precursor **2** was synthesised with an overall yield of 12%. Radiofluorination of **2** achieved radiochemically pure [^{18}F]**1** in 80 ± 13 min with a radiochemical yield of 20 ± 13% (decay-corrected) and molar activities up to 80 GBq/μmol (n=11). *In vitro*, cell associated activity of [^{18}F]**1** increased over one hour, and retention of [^{18}F]**1** dropped to 50% over two hours. [^{18}F]**1** uptake did not correlate with ATM expression, but could be reduced significantly with an excess of known ATM inhibitors, demonstrating specific binding of [^{18}F]**1** to ATM. *In vivo*, fast hepatobiliary clearance was observed with tumour uptake ranging 0.13-0.90%ID/g after one hour.

Conclusion: Here we report the first radiofluorination of an ATM inhibitor and its *in vitro* and *in vivo* biological evaluations, revealing the benefits but also some limitations of ^{18}F-labelled ATM inhibitors.

Introduction

Ataxia Telangiectasia Mutated (ATM) is a key mediator of the DNA damage response with a key role in maintaining genomic integrity, making it key in the study and therapy of cancer. When ATM is activated in the presence of double stranded DNA breaks (DSBs) resulting from genomic instability, replication stress, or external stimuli such as radio- or chemotherapy, it undergoes monomerization and autophosphorylation at S1981. Its key role in DNA damage repair signalling has led to a variety of ATM inhibitors (ATMi) being developed to reduce ATM enzymatic activity, restricting repair of harmful lesions and cell cycle arrest, resulting in mitotic catastrophe and cell death (table 1) [1, 2]. Although there are a handful of ATM inhibitors currently undergoing clinical trials, none have been approved for used in patients yet.

The study of ATM both mechanistically and as a therapeutic target has led to the development of a range of techniques to visualise ATM, recently reviewed [3]. Investigations into the activation mechanisms of ATM have historically used classical techniques such as immunoblotting to identify ATM activation and

the effects on downstream targets of ATM, aided by the used of increasingly selective ATM inhibitors. Due to the complexity of ATM mechanisms the study of proteins associated with ATM have also been used to assess its activity indirectly. One elegant example is the use of PET with ^{18}F-labelled FAC to image the expression of deoxycytidine kinase (dCK), an enzyme that is phosphorylated by ATM, activating its role in nucleotide salvage for DNA damage repair [4]. More recently, direct imaging of the biodistribution of an ATM inhibitor using a ^{11}C-labelled version, [^{11}C]AZD1390, has demonstrated that particular inhibitor's ability to cross the blood-brain barrier in a phase I clinical trial [5, 6].

Radiolabelled analogues of investigational drugs add enormous value for the study of pharmacokinetics, can aid preclinical development, and act as companion biomarkers assisting patient stratification [7]. PET/SPECT imaging with these radiopharmaceuticals can be used to non-invasively assess tumour/tissue uptake and aid dose calculations and scheduling for each patient prior to treatment with the therapeutic, assisting the move to more personalised medicine. [^{11}C]AZD1390 demonstrated some of these benefits, however the relatively short half-life of ^{11}C (20 min) does limit the clinical applicability of ^{11}C-labelled small molecules.

The need for an ATM inhibitor labelled with a radionuclide that correlates with the pharmacokinetics of the inhibitor itself led to this work to create the first ^{18}F-labelled ATM inhibitor, utilising fluorine-18 as a radioisotope with a longer decay half-life of 110 min. The compound was chosen from a series of ATM inhibitors reported by Baalam *et al.* that includes a number of highly potent and selective molecules containing fluoride moieties in their structures [8]. Based on the structures and ATM inhibition data reported in this series, we developed a synthetic route to access an ^{18}F-labelled ATM inhibitor, [^{18}F]**1** (figure 1). Herein we report the synthesis of a nitro-precursor molecule **2**, radiofluorination to afford [^{18}F]**1**, and biological assessment of [^{18}F]**1** *in vitro* and *in vivo,* investigating its potential as an ATM PET imaging agent.

Methods

Chemical Synthesis

The synthesis of the non-radioactive ^{19}F version of compound **1** followed methods reported by patent [8], with minor modifications as detailed in the supporting information (figure 2, supplementary figure S1). The synthesis of nitro-precursor **2** followed the same route as for [^{19}F]**1**. Full synthetic details are available in the supporting information.

Radiosynthesis

Radiosynthesis of [^{18}F]**1** was achieved through nucleophilic aromatic substitution (S_NAr) of **2** (1 mg) with [^{18}F]fluoride (5-12 GBq) dried azeotropically with acetonitrile in the presence of K_2CO_3 (6 mg) and $K_{2,2,2}$

(30 mg) reacting for 10 min at 120°C in DMF (figure 2). HPLC purification of [^{18}F]**1** was performed using a Luna 10u C18(2) 100 Å 250 x 10 mm semi-preparative column in 25:75 acetonitrile/0.1% formic acid aqueous buffer, followed by reformulation in 10% DMSO in 0.9% saline solution for *in vitro* and *in vivo* studies. Manual radiolabelling reactions were performed using aliquots of [^{18}F]fluoride (approx. 200 MBq) azeotropically dried with acetonitrile with addition of K_2CO_3 (1 mg) and $K_{2,2,2}$ (5 mg) before the subsequent labelling reactions. The radiosynthesis was fully automated on an Eckert & Ziegler Modular-Lab system (full description of setup available in the supporting information).

In vitro **evaluation**

H1299 non-small cell lung cancer cells, either wildtype, or stably transfected with short hairpin RNA for ATM (shATM) or GFP (shGFP, as a control) expression knockdown, were kindly gifted by Dr Anderson Ryan at the University of Oxford [9]. All cells were cultured at 37°C and 5% CO_2 in Dulbecco's Modified Eagle Medium (DMEM) supplemented with 10% Foetal Bovine Serum (FBS) (Gibco, USA), 2 mM L-glutamine, 100 units/mL penicillin and 100 µg/mL streptomycin (PSG) (Sigma Aldrich); knockdown cell lines were additionally supplemented with 0.5 µg/mL puromycin dihydrochloride (Merck Life Science, UK). Cells were originally purchased from ATCC, were authenticated by the provider and by STR profiling. Cells were tested regularly for the absence of mycoplasma contamination and were cultured for a maximum of 20 passages after resuscitation from liquid nitrogen storage.

Western blot analysis was performed to compare the total ATM expression between cell models, in addition to expression of phospho-ATM^{S1981} (pATM), phospho-KAP1^{S824} (pKAP1), and phospho-CHK2^{T68} (pCHK2) expression to assess the effect of irradiation and ATM inhibition on ATM catalytic activity. Cells were irradiated (4 Gy; 0.75 Gy/min) or sham-irradiated and incubated at 37°C for one hour before harvesting cells for lysis and blotting (full details in supporting information). Where required, inhibitors were added to cells at the stated concentration from DMSO stock solutions (reaching no greater than 10% DMSO final concentration) with incubation for one hour prior to irradiation/sham-irradiation. The following antibodies and dilutions were used in this work: Phospho-ATM S1981 (ab81292, 1:5000, Abcam); phospho-KAP1 S824 (ab133440, 1:10,000, Abcam); phospho-CHK2 T68 (#2661, 1:1000, Cell Signalling Technologies); Total ATM (ab32420, clone [Y170], 1:500, Abcam); Total KAP1 (ab10483, 1:1000, Abcam); Total CHK2 (05-649, 1:1000, Merck Millipore); HRP-conjugated Tubulin (ab197740, clone [YL1/2], 1:4000, Abcam); HRP-conjugated β-Actin (clone 13E5, 1:1000, Cell Signalling Technologies), HRP-conjugated anti-rabbit secondary (HAF008, 1:1000, R&D Systems); HRP-conjugated anti-mouse secondary (HAF007, 1:1000, R&D Systems). All blots were repeated on at least two separate occasions with new cell lysates for validation.

To assess cellular uptake of [^{18}F]**1**, aliquots of H1299 shATM or shGFP cells were plated with 1x10^5 cells per well in 24-well plates in 500 µL complete growth medium and incubated overnight to allow cells to adhere. Cell culture medium was removed, cells washed with PBS and media replaced with DMEM (no additives). Cells were irradiated (4 Gy; 0.75 Gy/min) or sham-irradiated and incubated for one hour before addition of [^{18}F]**1**, followed by incubation at 37°C and 5% CO_2 for the indicated time. Supernatant cell

culture medium was collected, and cells were washed twice with PBS, after which they were lysed with 0.1 M sodium hydroxide (200 µL) for 30 min. The amount of ^{18}F-activity associated with each fraction was determined using a Wizard2 Automatic Gamma Counter (PerkinElmer).

Retention assays followed the same procedure with a one-hour incubation of cell with [^{18}F]**1**, but after culture medium was aspirated and cells washed with PBS (2×500 µL), it was replaced (500 µL DMEM) and cells incubated at 37°C and 5% CO_2 for the desired time. The amount of ^{18}F-activity retained in cells was then determined as above.

Blocking studies followed the same procedure as uptake with one hour tracer incubation, however the replacement media contained the blocking agent at the indicated concentrations in no greater than 10% DMSO, and a DMSO control was also run in parallel at the highest DMSO concentration used, followed by incubation at 37°C and 5% CO_2 for one hour before irradiation.

In vivo **evaluation**

All animal procedures were performed in accordance with the UK Animals (Scientific Procedures) Act 1986 and with local ethical committee approval. Mice were bred from parent C57BL/6J mice heterozygous for a targeted mutation in the ATM^{tm1Awbl} allele to produce ATM$^{-/-}$ mice (Jackson laboratory). Wild type mice (ATM$^{+/+}$) from this breeding program were used as controls. In a separate study, tumour xenografts were created in BALB/c *nu/nu* mice (8-weeks old) via subcutaneous injection of H1299 wildtype, shATM knockdown, or shGFP knockdown cells on both sides of the hind flank. Total tumour volumes were allowed to reach an average of 600 mm^3 (range 330-930 mm^3) before imaging and/or biodistribution studies (approx. 6-10 weeks after inoculation).

Animals were anaesthetised by 4% isoflurane gas (0.5 L/min O_2) and maintained at approx. 2% and 37°C throughout the imaging session. C57BL/6 ATM$^{+/+}$ and ATM$^{-/-}$ mice were administered [^{18}F]**1** (83 ng; 0.5-4.6 MBq) via intravenous bolus injection in the lateral tail vein. Xenograft bearing BALB/c *nu/nu* mice were administered [^{18}F]**1** (0.5 µg; 0.7-9.6 MBq) via intravenous bolus injection to the lateral tail vein. PET/CT scanning was completed using a VECTor4CT scanner (MILabs, Utrecht, the Netherlands) for one hour and was immediately followed by culling, dissection and gamma counting of selected organs. Tumour tissue was immediately flash frozen in liquid nitrogen and mounted in OCT before producing 10 µm thick section for autoradiography and H&E staining. Alternatively, frozen tumour tissue was macerated and lysed in RIPA buffer for western blot analysis (full details available in the supporting information). Reconstruction of both CT and PET images was performed with the MILabs reconstruction analysis using a γ-ray energy window of 467–571 keV (background weight 2.5%), 0.8 mm^3 voxel size, 8 subsets and 5 iterations using the manufacturer's SROSEM reconstruction type. PET images were each registered to CT, attenuation corrected, calibrated by imaging a phantom containing a fluorine-18 standard solution, and analysed using PMod software package (Version 3.807, PMOD Technologies).

Statistical Analysis

Statistical analysis was performed using GraphPad Prism v9 (GraphPad Software, San Diego, CA, USA). In each case, a 1-way or 2-way ANOVA was performed with multiple comparisons using Šidák's test.

Results

The synthesis of reference compound [^{19}F]**1** was completed with an overall yield of 33% over 12 steps. Nitro-precursor **2** was prepared with a yield of 12% over 12 steps (figure 2, supplementary figure S1).

Reaction condition screening during manual radiofluorination of precursor **2** revealed the best chemical yield was obtained in DMF at 120°C for 10 min. The automated radiosynthesis of [^{18}F]**1**, performed on an Eckert & Ziegler Modular-Lab, was completed in 80 ± 13 min with a radiochemical yield of 20 ± 13% (decay-corrected), radiochemical purity >99% and molar activity up to 79.5 GBq/μmol (n=11) (figure 2, supplementary figure S2).

Western blot analysis confirmed a reduced total-ATM expression in the shATM knockdown H1299 cells compared to the shGFP knockdown H1299 cells, and reduced phospho-ATM^{S1981} (pATM) expression in irradiated shATM cells compared to irradiated shGFP cells. The expression of downstream targets of pATM, pKAP1 and pCHK2, were also reduced in the irradiated shATM knockdown cells compared to the irradiated shGFP knockdown cells. In irradiated shGFP knockdown cells, ATM inhibition with known ATM inhibitors AZD1390, [^{19}F]**1**, AZD0156, KU60019, as well as precursor **2**, were confirmed by a decrease in pATM, pKAP1, and pCHK2 expression relative to a DMSO control (figure 3).

Uptake of [^{18}F]**1** in cells showed an increase in cell associated activity over one hour followed by a plateau. Retention of [^{18}F]**1** in the same cells revealed a gradual decrease in cell associated activity of approximately 50% over two hours. No differences between cell associated activity were observed between the different cell lines/irradiation conditions. Nonetheless, significant blocking was observed with increasing concentrations of the ATM inhibitor KU60019, demonstrating some specific binding of [^{18}F]**1** to ATM and revealing high levels of non-specific uptake. Surprisingly, addition of some known ATM inhibitors AZD1390, AZD0156, or [^{19}F]**1** resulted in an initial blocking effect at lower concentrations of the inhibitor (0.1-10 nM), but an increase in cell-associated activity at higher concentrations (figure 4).

PET/CT imaging and *ex vivo* biodistribution of [^{18}F]**1** in wildtype and ATM-knockout C57BL/6 mice one hour after intravenous administration revealed hepatobiliary clearance (figure 5). Challenges due to [^{18}F]**1** adhering to the walls of long canula lines during intravenous injection meant that short canula lines were necessary to administer the dose, resulting in a delayed start of dynamic PET imaging (starting approx. 10 minutes after injection of the tracer) by which point tissue activity concentrations remained near constant, preventing pharmacokinetic analysis.

Biodistribution of [^{18}F]**1** in BALB/c *nu/nu* mice was comparable to C57BL/6 mice. Uptake in H1299 tumour xenografts was measured as 0.38 ± 0.12%ID/g (wildtype), 0.35 ± 0.14%ID/g (shGFP), and 0.35 ± 0.10%ID/g (shATM). No significant differences were observed in tumour uptake between the different

tumour types, reflecting our *in vitro* results, despite confirmation of xenograft ATM knockdown status by *ex vivo* western blot (supplementary figure S5). Autoradiography of tumour sections revealed heterogeneous uptake across the xenografts that was not specific to tumour type. H&E staining of the same tumour sections revealed regions of tissue lacking nuclei (possibly suggesting necrosis) that matched autoradiography low signal regions of the tumour, indicating uptake of the tracer only in viable cells (supplementary figure S6). The few tumours revealed to have necrotic centres did not have significantly different uptake (%ID/g) compared to the more viable tumours. Autoradiography analysis of viable cell regions (i.e., excluding areas of necrosis) revealed no significance in %ID/cm^2 between xenograft type (supplementary figure S7).

Discussion

ATM inhibitors are an up and coming treatment for cancer. While there are four inhibitors currently undergoing human trials (Table 1), none are currently approved for clinical use. A host of preclinical studies have demonstrated the potential of these inhibitors for cancer treatment, most in combination with other DNA damaging therapies [10, 11]. However, many drugs fail to reach or progress through this vital stage of drug development due to lack of understanding of the drug efficacy. Studying the pharmacokinetics of experimental drugs provides vital information that can aid the transition into clinical evaluation. Drug pharmacokinetics are generally measured through the sampling of blood, urine, and tissue biopsies over time, which can be invasive and cannot reveal drug biodistribution across the whole body or in heterogeneous tissues, or indeed the tumour target distribution.

The use of nuclear imaging can provide a clearer picture of drug pharmacokinetics across the whole body non-invasively with the use of radiolabelled drug analogues [7]. This technique can assist in designing treatment plans for patients (e.g. calculating drug dosage), but can also assist the clinical development of novel drugs. A radiolabelled ATM inhibitor promises to visualise and quantify drug distribution, while also having the potential to give insight into ATM tissue distribution. The previously reported [^{11}C]AZD1390 has shown in clinic studies how radiopharmaceuticals can aid these measurements, however the short half-life of ^{11}C reduces the scope of using ^{11}C-labelled drug variants due to the requirement of on-site cyclotrons in hospitals. Where the radiochemistry is available and able to retain drug properties, the use of ^{18}F-radiotracers can overcome this issue. Hence, we radiofluorinated potent ATM inhibitor **1**, as a tool to investigate ATM PET imaging.

Our *in vitro* model system demonstrated the ability of **1** to inhibit ATM activity through inhibition of ATM Serine-1981 phosphorylation and the phosphorylation of downstream targets of ATM, KAP1 and CHK2. This showed **1** to have ATM inhibitory properties comparable to other ATM inhibitors such as AZD1390, AZD0156, and KU60019, confirming its reported sub-nM IC_{50} value of ATM inhibition [8]. This data indicates that **1** binds to and inhibits ATM in live cells and reinforces the proposal that [^{18}F]**1** could be used to image ATM.

While some specific binding to ATM of [^{18}F]**1** was observed, as evident from statistically significant reductions of cell associated activity after exposure to an excess of the ATM inhibitor KU60019 ($P<0.001$), high levels of non-ATM specific cell association were also revealed. This relatively low level of ATM specific uptake relative to the non-specific uptake is likely due to the innately low cellular expression of ATM [12–14] which may lead to only slight observable changes in [^{18}F]**1** uptake, in addition to the highly lipophilic nature of the inhibitor which aides passive transport of the compound into the cell. This low ratio of specific to non-specific binding may be masking any differences in uptake that are expected between cell lines with highly varying ATM expression levels, as well as the effects of irradiation (and therefore increased expression of active, phosphorylated ATM) on the uptake of [^{18}F]**1**. This result demonstrates the limits of [^{18}F]**1** for mechanistic studies of ATM.

Surprisingly, blocking [^{18}F]**1** uptake with high molar excess (1000 nM) of the ATM inhibitors AZD1390, AZD0156, or [^{19}F]**1** resulted in an increase in cell associated activity of [^{18}F]**1**, compared to a DMSO control, despite demonstration by western blot that total ATM protein levels were not affected by the same doses of the blocking agents. Since ATM expression levels remain constant in these blocking conditions, it is not yet clear what caused this effect. Quinoline-based ATM inhibitors are highly lipophilic compounds, so it may be hypothesised that at high concentrations the blocking compounds could be altering cell membrane permeability, increasing cellular infiltration of [^{18}F]**1**. Alternatively, the blocking agents may be impacting the expression of other kinases unrelated to ATM expression, resulting in increased off-target specific binding of [^{18}F]**1**.

Although murine ATM is different to human ATM [15], it retains much of the same structure, and many of the same phosphorylation sites, and we were able to demonstrate murine ATM inhibition (and reduction of downstream target pKAP1) by **1** using western blot (Supplementary figure S7). *In vivo*, the comparison in biodistribution of [^{18}F]**1** in wildtype versus ATM-knockout mice showed significant differences in the liver and kidney uptake (figure 5). Given the observed hepatobiliary and renal clearance (demonstrated by high uptake in the liver, small intestine, and kidneys), it may be hypothesised that the lower uptake in these organs of the wildtype mice could be due to an 'ATM sink' effect, where there may be increased specific binding of [^{18}F]**1** to ATM across the rest of the body, slowing the hepatobiliary clearance (therefore reducing hepatobiliary organ uptake of [^{18}F]**1**) relative to the ATM-knockout mice. Alternatively, this difference could be due to fundamental differences in metabolism between the two mouse strains, i.e., ATM$^{+/+}$ vs. ATM$^{-/-}$. It should be noted that the ATM$^{-/-}$ knockout mice were of smaller size and weight than wildtype mice, although *ex vivo* organ weight as a percentage of body weight was comparable.

Similar hepatobiliary clearance of [^{18}F]**1** was observed in xenograft-bearing BALB/c *nu/nu* mice, but there was no significant difference between uptake in any of the organs or tumours across the different tumour models. This lack of differential uptake in the H1299 tumour xenografts mimics our *in vitro* uptake results in the same cells, indicating that the use of a radiolabelled ATMi for imaging ATM status may be challenging in a clinical setting, but still demonstrates the usefulness of [^{18}F]**1** to non-invasively measure whole body drug biodistribution and quantify tumour-drug uptake.

Conclusions

To the best of our knowledge, radiolabelled compound [^{18}F]**1** is the first reported radiofluorinated ATM inhibitor. We were able to demonstrate the cellular uptake of [^{18}F]**1** *in vitro*, and revealed the challenges in determining specific binding to ATM, likely due to low ATM expression in cells in comparison to a high non-specific uptake. *In vivo*, no significant difference in uptake between tumour xenografts expressing different levels of ATM was observed, but we were able to demonstrate whole body drug biodistribution and the hepatobiliary clearance of [^{18}F]**1**. Taken together, these results show the potential challenges in using radiotracers to assess ATM status, but highlight the potential benefit of developing similar radiofluorinated ATM inhibitors for the non-invasive assessment of drug pharmacokinetics and tumour distribution.

Statements And Declarations

Funding

This research was supported by MRC (MR/R01695X/1) and CRUK though the Oxford Institute for Radiation Oncology. The authors disclose no potential conflicts of interest.

Competing Financial Interests

The authors have no relevant financial or non-financial interests to disclose.

Author contributions

All authors contributed to the study concept and design. Material preparation, data collection and analysis were performed by Claudia Fraser, Javier Ajenjo, Mathew Veal, Gemma Dias, Kathy Chan, Edward O'Neill, Doreen Lau, Gianluca Destro and Anna Pacelli. The first draft of the manuscript was written by Claudia Fraser and all authors commented on previous versions of the manuscript. All authors read and approved the final manuscript.

References

1. Minchom A, Aversa C, Lopez J. Dancing with the DNA damage response: next-generation anti-cancer therapeutic strategies. Ther Adv Med Oncol. 2018;10:1758835918786658. https://doi.org/10.1177/1758835918786658.
2. Kantidze OL, Velichko AK, Luzhin AV, Petrova NV, Razin SV. Synthetically Lethal Interactions of ATM, ATR, and DNA-PKcs. Trends Cancer. 2018;4(11):755–68. https://doi.org/10.1016/j.trecan.2018.09.007.
3. Huang C, Filippone NR, Reiner T, Roberts S. Sensors and Inhibitors for the Detection of Ataxia Telangiectasia Mutated (ATM) Protein Kinase. Mol Pharm. 2021;18(7):2470–81. https://doi.org/10.1021/acs.molpharmaceut.1c00166.

4. Bunimovich YL, Nair-Gill E, Riedinger M, et al. Deoxycytidine kinase augments ATM-Mediated DNA repair and contributes to radiation resistance. PLoS One. 2014;9(8):e104125. https://doi.org/10.1371/journal.pone.0104125.
5. Durant ST, Zheng L, Wang Y, et al. The brain-penetrant clinical ATM inhibitor AZD1390 radiosensitizes and improves survival of preclinical brain tumor models. Sci Adv. 2018;4(6):eaat1719. https://doi.org/10.1126/sciadv.aat1719.
6. Jucaite A, Stenkrona P, Cselényi Z, et al. Brain exposure of the ATM inhibitor AZD1390 in humans-a positron emission tomography study. Neuro Oncol. 2021;23(4):687–96. https://doi.org/10.1093/neuonc/noaa238.
7. Fischman AJ, Alpert NM, Rubin RH. Pharmacokinetic imaging: a noninvasive method for determining drug distribution and action. Clin Pharmacokinet. 2002;41(8):581–602. https://doi.org/10.2165/00003088-200241080-00003.
8. Barlaam B, Eatherton A, Hunt T, Pike K. 2017. 8-[6-[3-(amino)propoxy]-3-pyridyl]-1-isopropyl-imidazo[4,5-c]quinolin-2-one derivatives as selective modulators of ataxia telangiectasia mutated (ATM) kinase for the treatment of cancer. WO2017046216A1.
9. Weber AM, Drobnitzky N, Devery AM, et al. Phenotypic consequences of somatic mutations in the ataxia-telangiectasia mutated gene in non-small cell lung cancer. Oncotarget. 2016;7(38):60807–22. https://doi.org/10.18632/oncotarget.11845.
10. Weber AM, Ryan AJ. ATM and ATR as therapeutic targets in cancer. Pharmacol Ther. 2015;149:124–38. https://doi.org/10.1016/j.pharmthera.2014.12.001.
11. Batey MA, Zhao Y, Kyle S, et al. Preclinical evaluation of a novel ATM inhibitor, KU59403, in vitro and in vivo in p53 functional and dysfunctional models of human cancer. Mol Cancer Ther. 2013;12(6):959–67. https://doi.org/10.1158/1535-7163.MCT-12-0707.
12. Bekker-Jensen DB, Kelstrup CD, Batth TS, et al. An Optimized Shotgun Strategy for the Rapid Generation of Comprehensive Human Proteomes. Cell Syst. 2017;4(6):587–99.e4; https://doi.org/10.1016/j.cels.2017.05.009.
13. Beck M, Schmidt A, Malmstroem J, et al. The quantitative proteome of a human cell line. Mol Syst Biol. 2011;7:549. https://doi.org/10.1038/msb.2011.82.
14. Wiśniewski JR, Hein MY, Cox J, Mann M. A "proteomic ruler" for protein copy number and concentration estimation without spike-in standards. Mol Cell Proteomics. 2014;13(12):3497–506. https://doi.org/10.1074/mcp.M113.037309.
15. Daniel JA, Pellegrini M, Lee JH, Paull TT, Feigenbaum L, Nussenzweig A. Multiple autophosphorylation sites are dispensable for murine ATM activation in vivo. J Cell Biol. 2008;183(5):777–83. https://doi.org/10.1083/jcb.200805154.
16. A Study to. Assess the Safety and Tolerability of AZD1390 Given With Radiation Therapy in Patients With Brain Cancer. ClinicalTrials.gov Identifier: NCT03423628.
17. A Platform Study of Novel Agents in. Combination With Radiotherapy in NSCLC (CONCORDE). ClinicalTrials.gov Identifier: NCT04550104.

18. Pike KG, Barlaam B, Cadogan E, et al. The Identification of Potent, Selective, and Orally Available Inhibitors of Ataxia Telangiectasia Mutated (ATM) Kinase: The Discovery of AZD0156 (8-{6-[3-(Dimethylamino)propoxy]pyridin-3-yl}-3-methyl-1-(tetrahydro-2 H-pyran-4-yl)-1,3-dihydro-2 H-imidazo[4,5- c]quinolin-2-one). J Med Chem. 2018;61(9):3823–41. https://doi.org/10.1021/acs.jmedchem.7b01896.
19. Study to Assess the. Safety and Preliminary Efficacy of AZD0156 at Increasing Doses Alone or in Combination With Other Anti-cancer Treatment in Patients With Advanced Cancer (AToM). ClinicalTrials.gov Identifier: NCT02588105.
20. First-in-human Study of M4076 in Advanced Solid Tumors (DDRiver Solid Tumors 410). ClinicalTrials.gov Identifier: NCT04882917.
21. Fuchss T, Becker A, Kubas H, Graedler U. Imidazolonylquinoline compounds and therapeutic uses thereof. WO2020193660A1; 2020.
22. M3541 in. Combination With Radiotherapy in Subjects With Solid Tumors. ClinicalTrials.gov Identifier: NCT03225105.
23. Golding SE, Rosenberg E, Valerie N, et al. Improved ATM kinase inhibitor KU-60019 radiosensitizes glioma cells, compromises insulin, AKT and ERK prosurvival signaling, and inhibits migration and invasion. Mol Cancer Ther. 2009;8(10):2894–902. https://doi.org/10.1158/1535-7163.MCT-09-0519.
24. Evaluation of a Promising. New Combination of Protein Kinase Inhibitors on Organotypic Cultures of Human Renal Tumors (COMBOREIN). ClinicalTrials.gov Identifier: NCT03571438.
25. Hickson I, Zhao Y, Richardson CJ, et al. Identification and characterization of a novel and specific inhibitor of the ataxia-telangiectasia mutated kinase ATM. Cancer Res. 2004;64(24):9152–9. https://doi.org/10.1158/0008-5472.CAN-04-2727.
26. Rainey MD, Charlton ME, Stanton RV, Kastan MB. Transient inhibition of ATM kinase is sufficient to enhance cellular sensitivity to ionizing radiation. Cancer Res. 2008;68(18):7466–74. https://doi.org/10.1158/0008-5472.CAN-08-0763.
27. Development of a cell-based, high-throughput screening assay for ATM kinase inhibitors [published correction appears in J Biomol Screen. 2014 Dec;19(10):1418]. *J Biomol Screen*. 2014;19(4):538-546; https://doi.org/10.1177/1087057113520325.

Table

Table 1 is available in the Supplemental Files section.

Figures

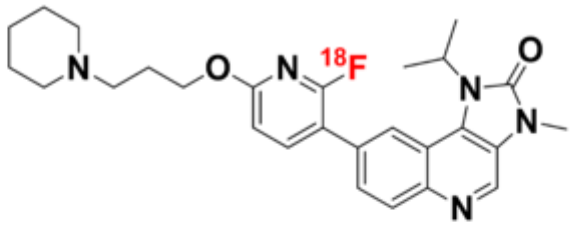

[18F]**1**

Cellular IC_{50} by catalytic inhibition reported for [19F]**1**	**ATM**	**< 0.00043 µM**
	ATR	> 30 µM
	PI3K	5.75 µM
	mTOR	> 5.19 µM

Figure 1

Target compound [18F]**1** and reported inhibitory data

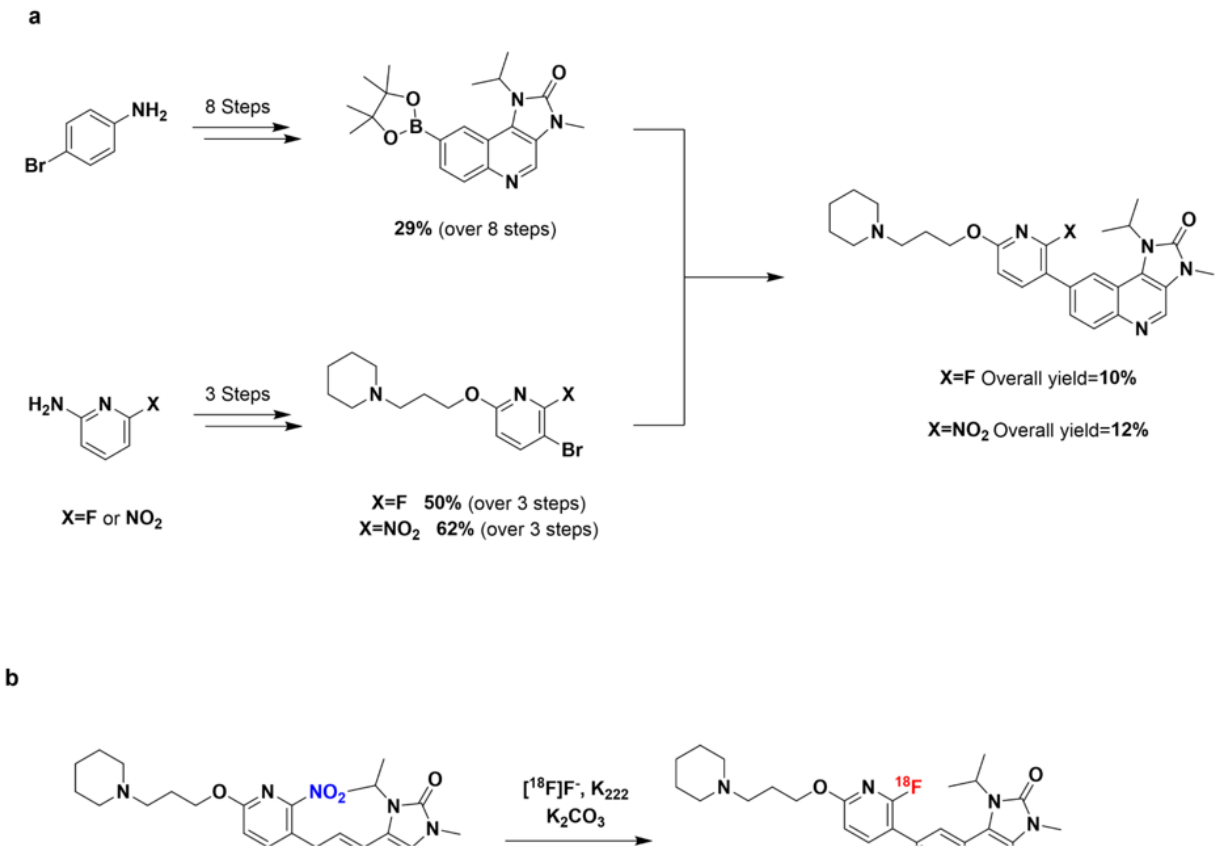

Figure 2

(a) Synthetic pathway to reference [^{19}F]**1** and nitro-precursor **2**. (b) Radiosynthesis of [^{18}F]**1** from **2**

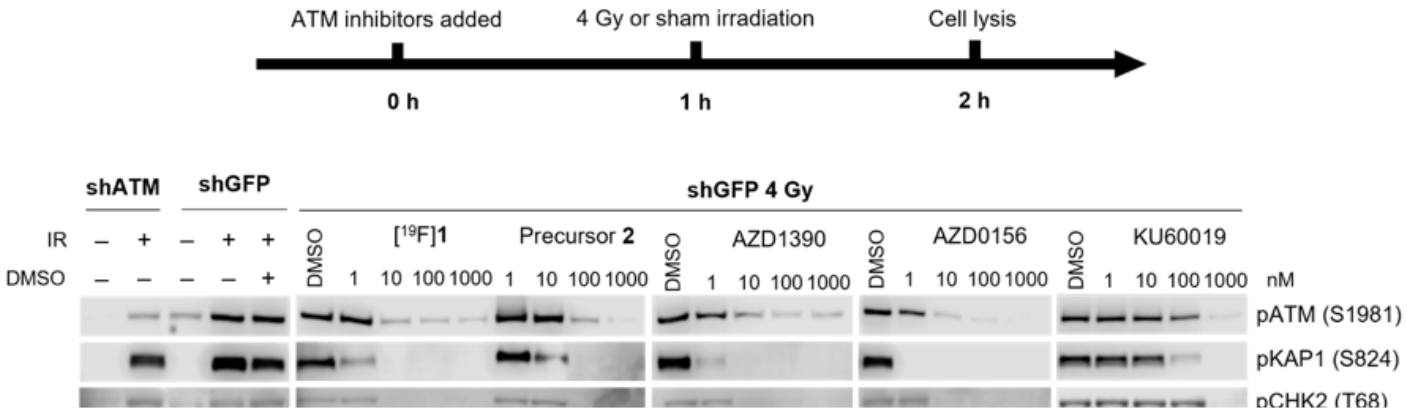

Figure 3

Higher ATM expression is observed in H1299 shGFP knockdown cells compared to H1299 shATM knockdowns. Irradiation of cells (4 Gy) causes an increased expression of pATM, pKAP1, and pCHK2. A decrease in expression of pATM and downstream targets pKAP1 and pCHK2 is observed following treatment of shGFP (4 Gy) cells with different ATM inhibitors

Figure 4

(a) Cell uptake and (b) retention of [^{18}F]**1** in H1299 shATM and shGFP cells. (c) Cell associated activity in H1299 shATM and shGFP cells after pre-treatment with a range of ATM inhibitors (block)

Figure 5

Biodistribution of [^{18}F]**1** in C57BL/6 ATM-wildtype and ATM-knockout mice, 1 h after intravenous administration. Below show representative PET/CT MIP images demonstrating the hepatobiliary uptake of tracer in both wildtype and ATM-null mice

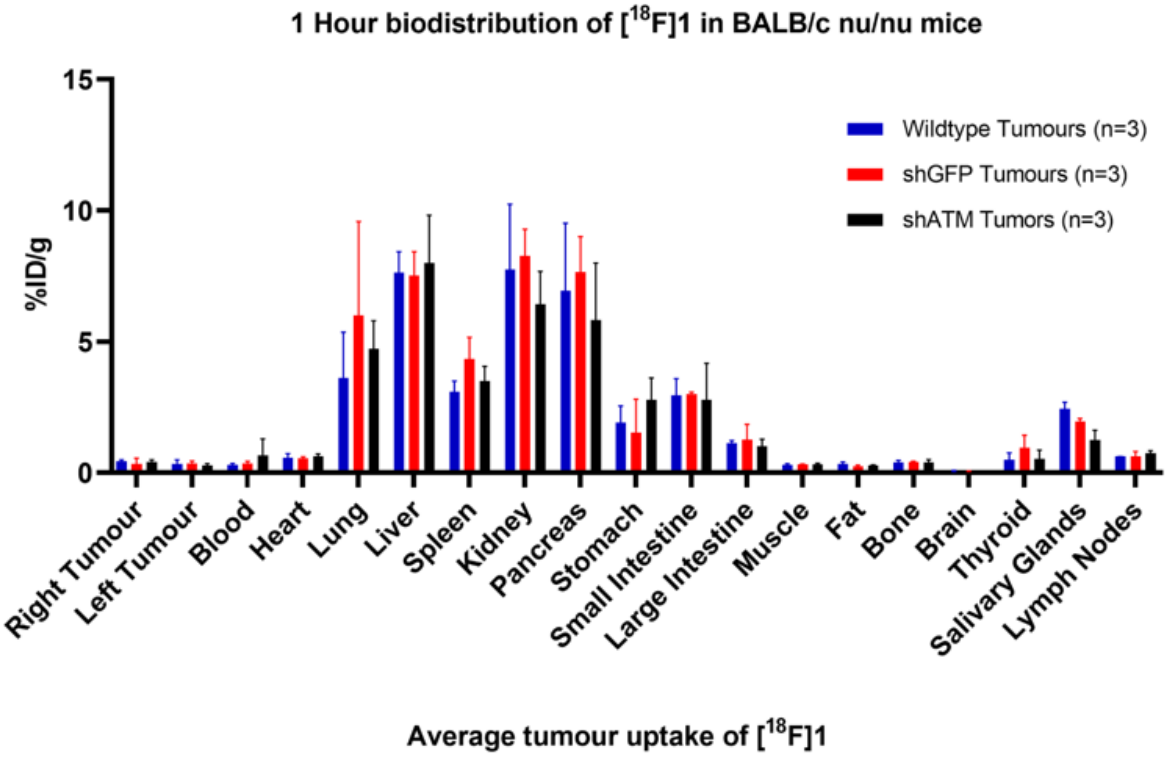

Figure 6

In vivo biodistribution of [^{18}F]**1** in BALB/c nu/nu mice bearing subcutaneous H1299 wildtype, shATM, or shGFP xenografts

Supplementary Files

This is a list of supplementary files associated with this preprint. Click to download.

- Table1.docx
- Fraseretal.Supportinginformation.pdf